Jurnal Teknologi, 45(D) Dis. 2006: 167–180
© Universiti Teknologi Malaysia

WELD EXTRACTION FROM DIGITISED RADIOGRAPHS USING GRAPHICAL ANALYSIS OF WELD INTENSITY PROFILES

SOO SAY LEONG[1], ZAHURIN SAMAD[2], MANI MARAN RATNAM[3] & MOHD ASHHAR KHALID[4]

Abstract. This paper presents an effective method to automatically extract welds from digitised radiographs. An algorithm was developed to locate and extract welds from the intensity profiles taken across the image by using a simple graphical analysis method. The algorithm proposed was successfully applied to extract welds from 45 digitised weld radiographic images. The proposed method of weld segmentation was found work well with radiographs having non-Gaussian intensity distribution across the weld region.

Key words: Nondestructive testing, weld radiograph, weld extraction.

Abstrak. Kertas kerja ini membentangkan suatu kaedah yang berkesan untuk menyari kimpalan secara automatik daripada radiograf yang telah didigitkan. Suatu algoritma untuk menentukan kedudukan dan menyari kimpalan daripada profil keamatan melintasi imej dengan menggunakan kaedah analisis grafik yang mudah telah dibangunkan. Algorithma tersebut telah diaplikasi untuk menyari kimpalan daripada 45 imej radiograf yang didigitkan. Kaedah segmentasi kimpalan yang dicadangkan didapati beroperasi dengan baik pada radiograf yang mempunyai taburan keamatan melintasi kawasan kimpalan.

Kata kunci: Ujian takmusnah, radiografi kimpalan, penyarian kimpalan.

1.0 INTRODUCTION

Non-destructive testing (NDT) is a branch of engineering concerned with methods of detecting defects in objects without altering the object in any way [1]. Radiography testing (RT) is one of the most important, versatile and widely accepted NDT methods for inspection of weld structures [2]. RT involves the use of penetrating gamma or X-radiation to examine the weld defects and internal features.

[1-3] School of Mechanical Engineering, University Science of Malaysia, Engineering Campus, Sri Ampangan, 14300 Nibong Tebal, Seberang Perai Selatan, Penang, MALAYSIA.
[4] Intelligent Systems Group, Malaysia Institute of Nuclear Technology (MINT), 43650 Bangi, Selangor, MALAYSIA.
* *Corresponding author*: Tel.: +6-04-5996325. Fax: +6-04-5941025, e-mail: mmaran@eng.usm.my

Conventionally, weld radiographs are checked and interpreted by human experts. However, interpretation of weld radiographs by humans is very subjective, inconsistent, labor-intensive and sometimes biased [3]. Therefore, various automated inspection techniques for weld radiographs were attempted worldwide over the past years. An automatic weld quality inspection system comprises three main stages: (a) Weld extraction, (b) defect detection and (c) defect classification [4]. Since defects only exist in the weld, the extraction operations can avoid unproductive processing of the background when defect detection algorithms are applied.

Existing automatic weld extraction algorithms suffer from a number of setbacks. For instance, Lawson and Parker developed a Multi-layer Perceptron neural network to extract the weld region in radiographic images [5]. The network was trained with a single image showing a typical weld that is to be inspected, coupled with a very simple schematic weld "template". However, the use of only one image as a template to train the network limits the network to working correctly only on images having similar characteristics, such as contrast and intensity variation. Liao and Ni analyzed gray level profile of weld radiographs and proposed that intensity plot of weld looks more like Gaussian than any other objects in weld radiograph [3]. An object in the profile is defined as an area between two troughs associated with a peak. Peak and trough detection was based on the slope of the profile. Finally, the profile for each detected object was determined and profile that is most similar to a Gaussian plot is identified as the weld. A major drawback for this method is that the algorithm is only limited to weld profiles that have Gaussian-like intensity distribution.

Fuzzy logic classifier has also been used in weld extraction [6]. Features were extracted from the intensity profiles of the weld, and then inputted into fuzzy logic system. Fuzzy k-NN and fuzzy c-means algorithm were used as pattern classifiers to recognize each peak in the intensity profile as weld and non-weld. However, this method did not produce good results. It generated false alarm rate of 16.08% to 23.14% with fuzzy k-NN classifier and 55.48% to 80.40% when using fuzzy c-means classifier. Even after post-processing procedure, false alarm rate of 10.73% to 28.34% was reported.

The focus of the current work is to develop an effective alternative method to extract welds from radiographs regardless of the characteristics of intensity profile across the weld. This paper is divided into the following sections: Introduction, weld extraction methodology, extraction of Weld Region, results and discussion and, finally, conclusions.

2.0 WELD EXTRACTION METHODOLOGY

2.1 Weld boundary point detection on Gaussian-type profiles

Liao and Ni [3] proposed that intensity profile taken across the weld of a defect-free weld image has a bell shape that can be approximated by a Gaussian distribution curve. In order to compare an intensity profile with a Gaussian distribution curve, normalization operation was performed to the weld intensity profile by dividing the intensity of each pixel by the summation of the intensities of all the pixels of that intensity profile between the left and right trough. The normalized intensity profile can be approximated by the Gaussian equation given by:

$$y_g = \frac{1}{\sigma\sqrt{2\pi}} e^{-\frac{(x-\mu)^2}{2\sigma^2}} \tag{1}$$

where μ is the mean, σ is the standard deviation, x is the pixel number along j-direction and y is the intensity value of the pixel. According to Liao and Ni, the value of σ can be determined from the following relationship [3]:

$$\text{FWHM} = 2.35\sigma \tag{2}$$

where *FWHM* is the full width value at half maximum. *FWHM* value was computed by first identifying the maximum intensity of the profile, followed by finding the x-locations of the intensity plot at the half of maximum intensity. The distance of these two x-locations at the half maximum intensity is the *FWHM*. The details on how to perform normalization operation and determine the s and m value are given in the paper published by Liao and Ni [3].

One common feature that can be visually observed from the intensity profiles taken across the weld is that the weld boundary points are respectively located between two troughs of the profile, as shown in Figure 1. By locating these weld boundary points, the weld region can be extracted. In this work, a graphical method has been developed to locate the weld boundary points from a weld intensity profile.

The approximated Gaussian distribution has a function given by (1). Assume that a straight line is drawn from the first point $x = 0$ to the center $x = m$ of the estimated Gaussian distribution curve. The equation of this line is given by:

$$y_l = mx + c \tag{3}$$

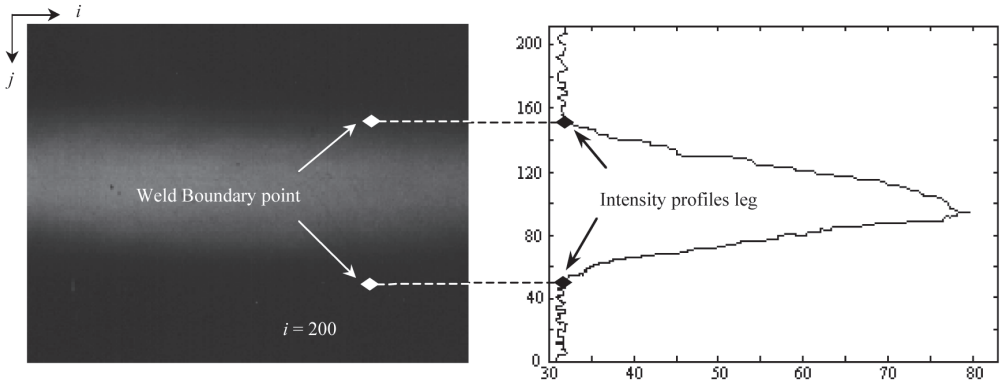

Figure 1 Weld boundary point location. (Source of weld radiograph: *International Institute of Welding)*

where m is the gradient while c is the interception on the intensity level axis. By substituting $x = 0$ and $x = m$ into (1), we have,

$$\text{at} \qquad x = x_1 = 0, \qquad y = y_1 = \frac{1}{\sigma\sqrt{2\pi}} e^{-\frac{\mu^2}{2\sigma^2}} \tag{4}$$

and

$$\text{at} \qquad x = x_2 = \mu, \qquad y = y_2 = \frac{1}{\sigma\sqrt{2\pi}} \tag{5}$$

From (1), when $x = 0$, $y = c$. Therefore, from (4):

$$c = \frac{1}{\sqrt{2\pi}} e^{-\frac{\mu^2}{2\sigma^2}} \tag{6}$$

The gradient, m can be obtained as:

$$m = \frac{y_2 - y_1}{x_2 - x_1} \tag{7}$$

By substituting x_1, x_2, y_1 and y_2 from Equation 4 and 5 into (7), we get:

$$\begin{aligned} m &= \left[\frac{1}{\sigma\sqrt{2\pi}} - \frac{1}{\sigma\sqrt{2\pi}} e^{-\frac{\mu^2}{2\sigma^3}}\right]\frac{1}{\mu} \\ &= \left[1 - e^{-\frac{\mu^2}{2\sigma^3}}\right]\frac{1}{\mu\sigma\sqrt{2\pi}} \end{aligned} \tag{8}$$

Therefore, (3) can be re-written as:

$$y_l = \left[1 - e^{-\frac{\mu^2}{2\sigma^2}}\right]\frac{x}{\mu\sigma\sqrt{2\pi}} + \frac{1}{\sigma\sqrt{2\pi}}e^{-\frac{\mu^2}{2\sigma^2}}$$
$$= \left\{\left[\left(1 - e^{-\frac{\mu^2}{2\sigma^2}}\right)\frac{x}{\mu}\right] + e^{-\frac{\mu^2}{2\sigma^2}}\right\}\frac{1}{\sigma\sqrt{2\pi}} \quad (9)$$

Subtracting (1) from (9) gives:

$$y = y_l - y_G = \left\{\left[\left(1 - e^{-\frac{\mu^2}{2\sigma^2}}\right)\frac{x}{\mu}\right] + e^{-\frac{\mu^2}{2\sigma^2}}\right\}\frac{1}{\sigma\sqrt{2\pi}} - \frac{1}{\sigma\sqrt{2\pi}}e^{-\frac{\mu^2}{2\sigma 2}}$$
$$= \frac{1}{\sigma\sqrt{2\sigma}}\left(\frac{x}{\mu} - \frac{x}{\mu}e^{-\frac{\mu^2}{2\sigma^2}} + e^{-\frac{\mu^2}{2\sigma^2}} - e^{-\frac{(x-\mu)^2}{2\sigma^2}}\right) \quad (10)$$

Equation (10) gives the vertical distance (in y-direction) of the Gaussian curve and the straight line drawn from $x = 0$ to $x = \mu$. This is illustrated in Figure 2, where the Gaussian curve, the straight line given by (3), and the distance between these two, known as distance plot and represented by (10), are illustrated. The Gaussian curve was plotted using $\sigma = 20$ and $\mu = 95$ for illustrative purpose. It was noticed that the weld boundary points for the estimated Gaussian curve could be determined by locating the corresponding x-location for maximum vertical distance on the distance plot given by (10) as shown in Figure 2.

According to Fermat's Theorem, if a function f has a local maximum or minimum at x, then $f'(x) = 0$ [7]. Thus, to determine the maximum value of $f(x)$ in (10), $f'(x)$ is set to zero. Hence:

$$0 = \frac{1}{\sigma\sqrt{2\pi}}\left(\frac{1}{\mu} - \frac{1}{\mu}e^{\frac{\mu^2}{2\sigma^2}} + \frac{x-\mu}{\sigma^2}e^{-\frac{(x-\mu)^2}{2\sigma^2}}\right) \quad (11)$$

Solving (11) gives two values for x, i.e. x_1 and x_2. By substituting these values into (10), we can obtain two values for y, i.e. y_1 and y_2. By finding the

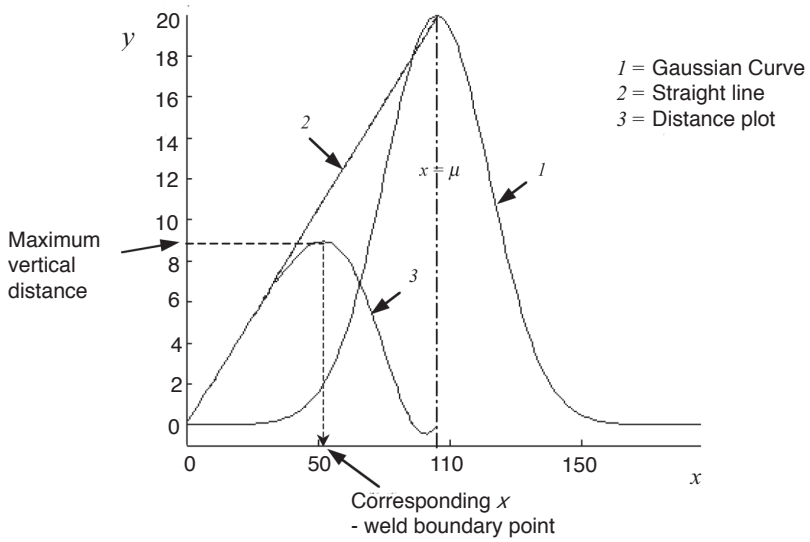

Figure 2 Gaussian plot, straight line and distance plot

corresponding x-location for maximum y in the distance plot, the weld boundary points can be located. This is the theory underlying the proposed work.

In an intensity profile taken across the weld in a radiograph, there will be two weld boundary points, an upper boundary point and a lower boundary point. In order to locate both boundary points, the distance plot was divided into two portions: left portion and right portion. The left portion is located from $x=0$ (first point of the profile) to $x=\mu$ (peak location of the profile), and was used to determine the weld upper boundary point. The right portion was located from $x=\mu$ to the last point of the profile, and was used to determine the weld lower boundary point. The corresponding x-location of the maximum y-value from each portion of difference plot is defined as the location for upper and lower weld boundary points respectively, as shown in Figure 3. Thus, weld boundary points for this intensity profile can be determined in this manner.

2.2 Weld boundary point detection on general intensity profiles

The weld boundary detection methodology was applied to an intensity profile taken from a defect-free weld radiograph, as shown in Figure 4(a)–(c). It was noticed that weld upper and lower boundary can be located correctly from this profile using the weld boundary points detection method proposed.

When an intensity profile is taken across a weld defect, however, the bell-shape intensity distribution will be distorted compared to that of a good weld profile. Figure 5(a) shows an example of a defective weld radiograph, where a

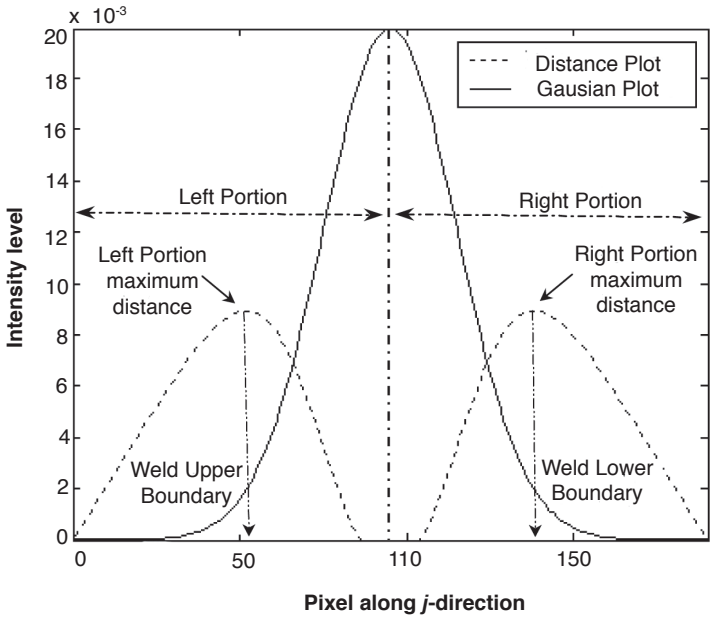

Figure 3 Weld upper and lower boundary point detection on Gaussian curve

(a) Intensity profile accorss weld

(b) Boundary points detected on image

crack is located at the middle of the weld. The intensity profile taken across the weld and crack defect is shown in Figure 5(b). The crack defect causes a valley on the profile and alters the Gaussian shape intensity profile. Distortion of intensity profile caused by the defect will produce an error in the detection of weld boundary points.

The weld intensity profile was divided into left and right portion at the location of the pixel with maximum intensity. The algorithm searches for maximum intensity from the left and right portions of the profile. Locations of pixels with maximum intensity on the distance plot in the left and right portion are regarded as the weld lower and upper boundary points. However, if a valley is present in the intensity profile, it creates a false peak in the distance plot. If the false peak intensity is higher than the true peak (which is associated to the weld boundary point), the algorithm developed will take this false peak as weld boundary points.

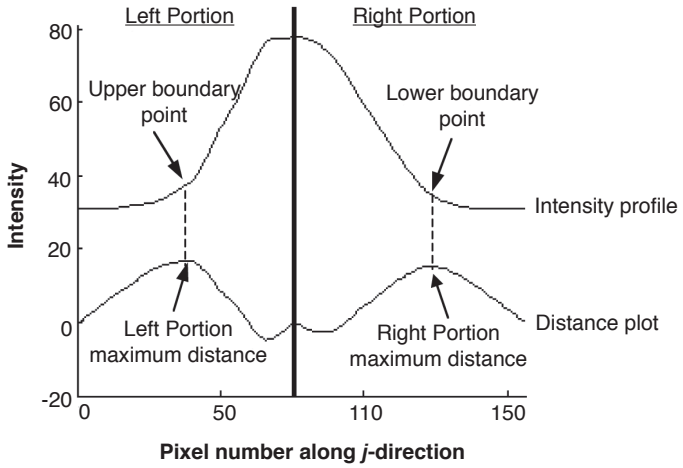

(c) Weld boundary detection from intensity profile across weld

Figure 4 Weld boundary point detection on intensity profile

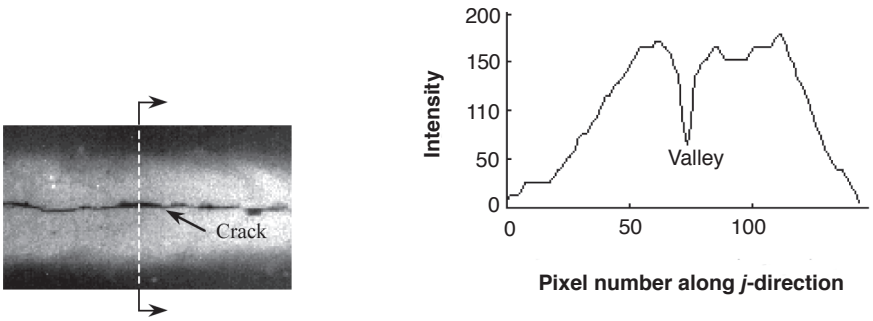

(a) Crack defect

(b) Intensity profile of crack defect

Figure 5 Intensity profile taken across crack defect

Figure 6 shows the false detection of weld boundary point across defective area of a weld radiograph. Since the vertical distance at the valley has the highest value in the left portion of the subtracted profile, it will be regarded as the weld lower boundary point, as shown in Figure 6(a). However, since there is no valley present in the right portion of the profile, weld upper boundary point was successfully located. Figure 6(b) shows the detected weld boundary points on weld radiograph. It can be observed that the location of weld lower boundary point is incorrect, where the location of the defect is incorrectly detected as weld lower boundary point.

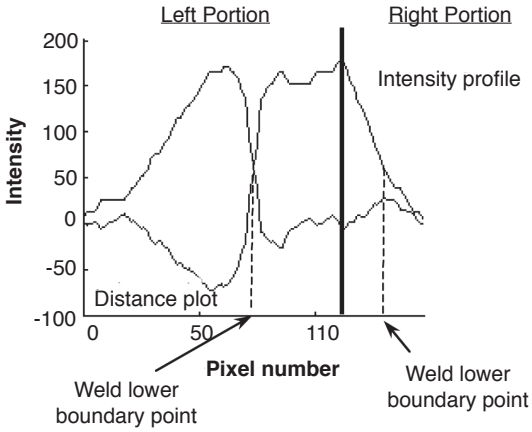

(a) Detection of false peak

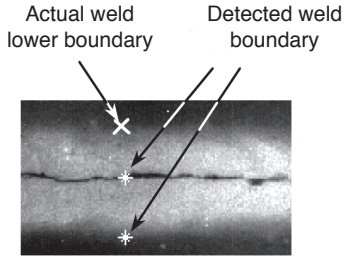

(b) Actual and detected boundary points

Figure 6 False detection of boundary points on defective area

In order to overcome this problem, the profile was divided into three different portions: left portion, right portion and weld region. To do this, half maximum of the intensity profile was determined first. Half maximum in the intensity profile is the location where the value of pixel intensity is equal to half of the maximum intensity in the profile. An example of this is illustrated in Figure 7(a). The maximum intensity is equal to 182; therefore half maximum for this profile is located at pixels with intensity value equal to 91. Left portion is defined as area from the first pixel on the profile to the first half maximum pixel while right portion is defined as the area from last half maximum pixel to the last pixel on the profile, as shown in Figure 7(a). The pixels located between left and right portion will be regarded as the weld region.

Therefore, unlike previous method where the left and right portion is divided at the pixel with maximum intensity, the new method divides the left and right portions at pixel having half maximum intensity. By doing this, false peak in the distance plot which is caused by defect can be avoided. The new algorithm searches for maximum value in the newly defined left and right portions. Maximum value of distance plot in left and right portion was selected as the lower and upper weld boundary point for intensity profile. Finally, location of maximum value on distance plot in each portion was selected as lower and upper boundary point accordingly. Image shown in Figure 7(b) shows that the weld upper and lower boundary points were detected correctly with this algorithm, even in the present of crack defect.

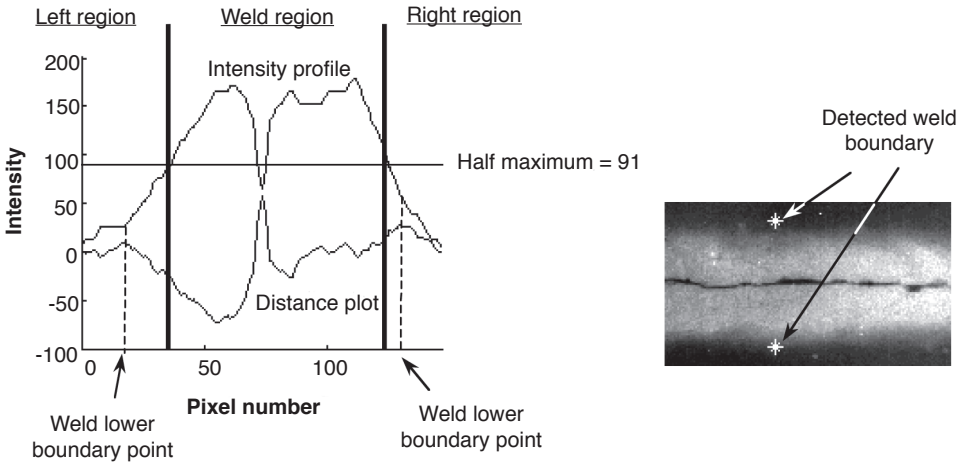

(a) Modifield half maximum algorithm (b) Detected boundary point

Figure 7 Weld boundary points detection on intensity profile taken across crack defect with modifield algorithm

3.0 EXTRACTION OF WELD REGION

The foregoing discussion on the detection of weld boundary points is only based on a single gray level profile. For a weld radiograph with a size of 573 × 224 pixels as shown in Figure 8(a) there are a total of 573 intensity profiles in *i*-direction. Each profile will generate its own upper and lower weld boundary points, as shown in Figure 8(b). These boundary points were joined to form the weld upper boundary and weld lower boundary respectively. The pixels located between the weld upper boundary and weld lower boundary were segmented as the weld.

4.0 RESULTS AND DISCUSSIONS

Intensity profile taken across defect-free area of a weld shows the characteristic of Gaussian curve [3]. Figure 9(a) shows examples of weld extraction across defect-free area with Gaussian-like intensity profile and defective area with non-Gaussian intensity profile.

Weld extraction process was successfully carried out on this image as shown in Figure 9(d). Weld upper and lower boundaries were detected correctly using the weld extraction methodology developed in this research. Figure 9(b) shows the Gaussian-like intensity profile of defect-free area in the image shown, which is taken across *a-a* in Figure 9(a). On the other hand, intensity profile taken

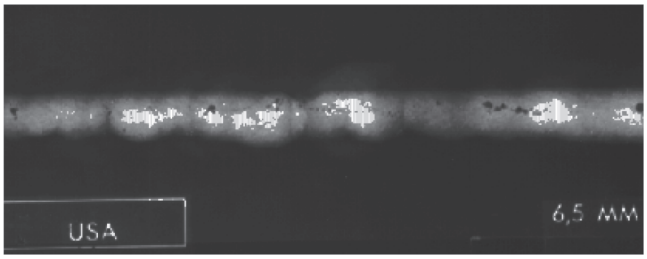

(a) A 224 X 573 pixels Weld radiograph

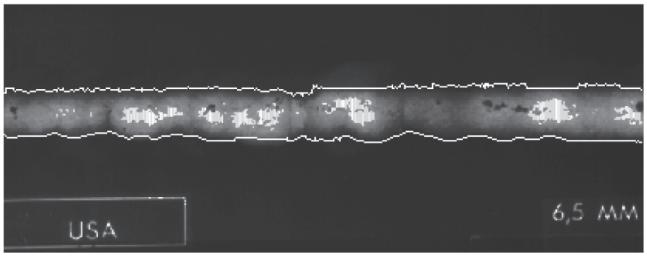

(a) A 224 X 573 pixels Weld radiograph

Figure 8 Results of weld extraction

repaired weld or defective area does not show the bell shape of a Gaussian plot [8]. Figure 9(c) shows an example of an intensity profile taken across defective area with non-Gaussian characteristic, which is taken across *b-b* in Figure 9(a). However, the technique proposed was able to extract the weld region from a non-Gaussian intensity profile as shown in Figure 9(d). Figures 10(a)–(e) show several weld images with defects where the weld boundaries were successfully detected.

Although the weld boundaries have been detected successfully as illustrated in Figures 10(a)-(e), the weld region detected in each case can be considered 'conservative'. This is because the proposed algorithm detects weld boundary points based on the maximum values in the distance plots. The limitation of this technique of detecting weld boundaries is that it is not possible to detect the boundary points if there are defects close to the weld edges, such as undercuts or cracks. Since most weld defects in the literature occur well inside the weld boundaries, the proposed algorithm can be applied in a practical situation for automated weld radiograph inspection.

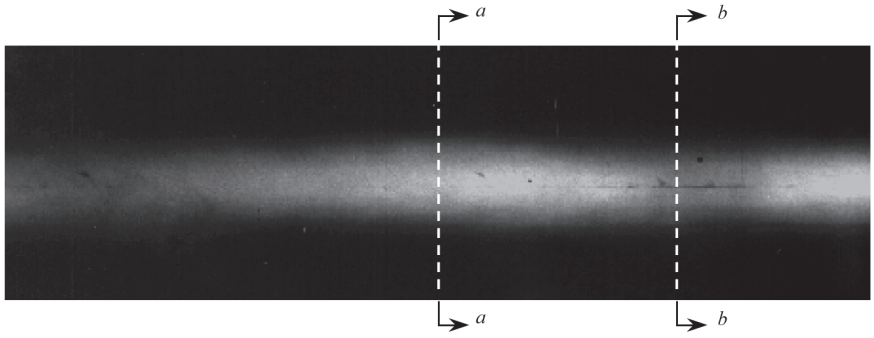

(a) Weld extraction across defect-free and defective area

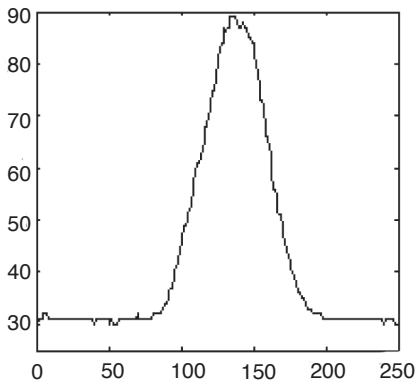

(b) Intensity profile across *a-a*

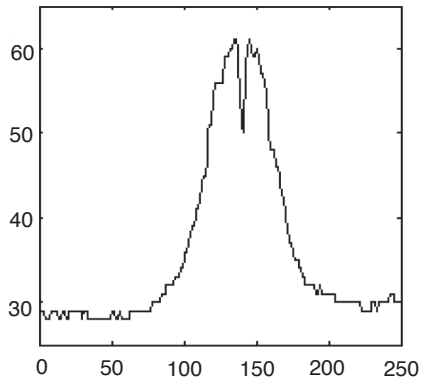

(c) Intensity profile across *b-b*

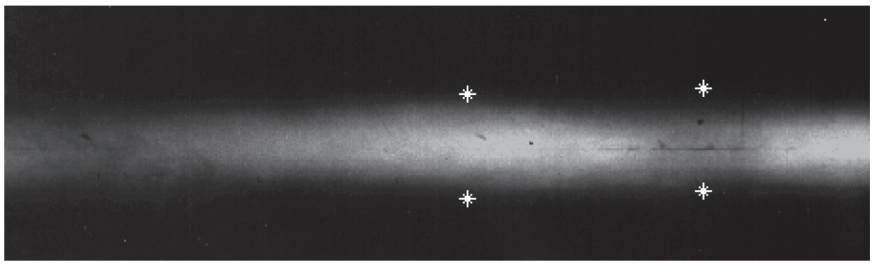

(c) Weld extraction result across defect-free and defective area

Figure 9 Weld extraction on weld radiograph with Gaussian-like and non-Gaussian intensity profile

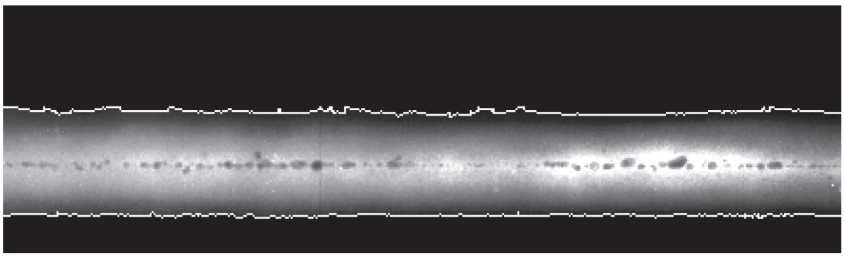

(a) Cavities

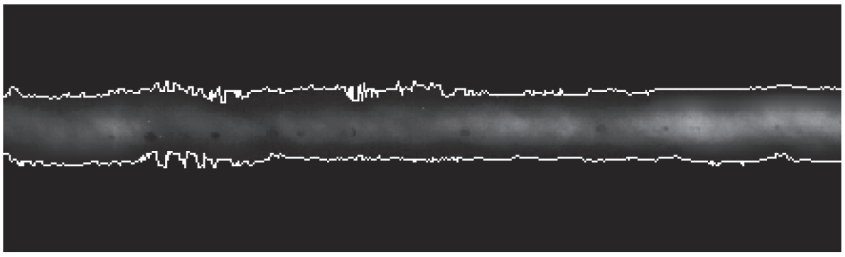

(b) Porosity

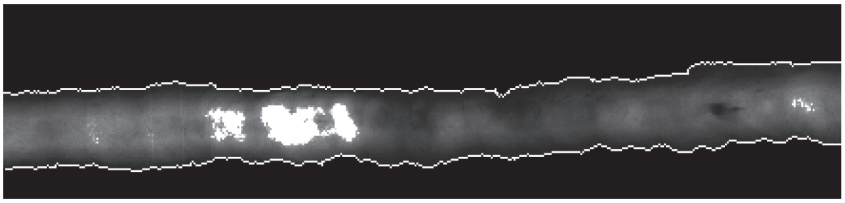

(c) Root cave

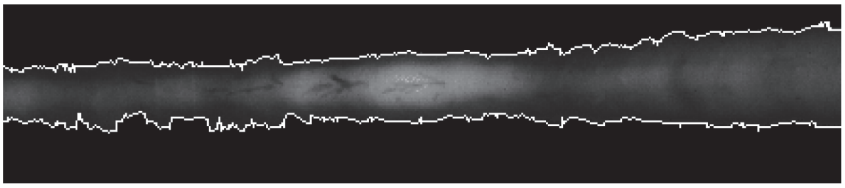

(d) Worm

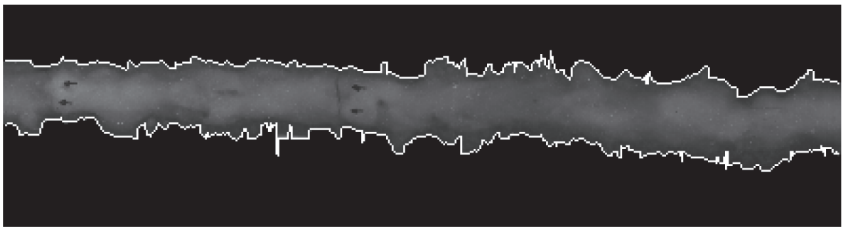

Figure 10 Various weld radiographs with detected weld boundaries

5.0 CONCLUSION

The methodology proposed by Liao and Ni [3] was based on the Gaussian characteristic of gray level profile taken across the weld area. Intensity profiles taken across weld defect, however, usually have non-Gaussian characteristic intensity profile. The false alarm rate in weld extraction reported by the authors for non-Gaussian profile weld is expected because their methodology was based on Gaussian characteristics.

The methodology proposed in this work is able to process weld radiographs having Gaussian-type as well as non-Gaussian characteristic gray level profiles. An algorithm to locate weld boundary points from weld intensity profile through a series of graphical analysis of intensity profile has been developed. This methodology was found to be able to extract welds from radiographs regardless of the characteristics of the intensity profiles. In addition, the proposed weld extraction methodology can also effectively segment the weld from the radiograph in the presence of various defect types at different locations within the weld region in the image.

ACKNOWLEDGEMENT

The authors would like to thank the Ministry of Science, Technology and Innovation for the offer of the IRPA Grant (Project No. 03-02-05-2190EA005) that has resulted in this research.

REFERENCES

[1] Lawrence, E.B. 1985. *Nondestructive Testing Handbook. Radiography and Radiation Testing.* Vol. 3. American Society for Nondestructive Testing.
[2] Hayes, C. 1997. The ABC's of Nondestructive Weld Examination. *Welding Journal* 76(5): 46-51.
[3] Liao, T.W. and J. Ni. 1996. An Automated Radiographic NDT System for Weld Inspection. Part I. Weld Extraction. *NDT&E Int.* 29(3): 157-162.
[4] Liao, T.W. 2003. Classification of Welding Flaw Types with Fuzzy Expert Systems. *Expert Systems with Applications* 25: 101-111.
[5] Lawson, S.W. and G.A. Parker. 1994. Intelligent Segmentation of Industrial Radiographs Using Neural Networks. *Proceeding of SPIE* 2347: 224-255.
[6] Liao, T.W., D.M. Li and Y.M. Li. 2000. Extraction of Welds From Radiographic Images Using Fuzzy Classifiers. *Information Sciences* 126: 21-40.
[7] Steward J. 2001. *Calculus: Concepts and Contexts.* 2nd Edition. Thomson Learning, Boston (USA).
[8] Liao, T.W. and Y.M. Li. 1998. An Automated Radiographic NDT System for Weld Inspection. Part II: Flaw detection. *NDT & E International* 31(3): 183-192.